Asymmetry and long-range character of lattice deformation by neutral oxygen vacancy in α-quartz

Vladimir B. Sulimov,[1] Peter V. Sushko,[1] Arthur H. Edwards,[2] Alexander L. Shluger,[1] and A. Marshall Stoneham[1]
[1]*Department of Physics & Astronomy, University College London, Gower St., London, WC1E 6BT, United Kingdom*
[2]*Air Force Research Laboratory, Space Vehicles Directorate, 3550 Aberdeen Ave. SE, KAFB, New Mexico 87117-5776*
(Received 3 October 2001; revised manuscript received 5 February 2002; published 10 July 2002)

The neutral oxygen vacancy in SiO_2 is important both through its role in controlled refractive index changes and as an archetypal intrinsic defect. We have studied the very significant effects of lattice relaxation on the structure and properties of this defect in both pure and Ge-doped α-quartz using a hybrid classical–*ab initio* embedded-cluster method. The neutral vacancy induces very strong and anisotropic lattice distortion. At the vacancy site, the Si-Si distance in α-quartz relaxes to the same spacing as in elemental Si. The long-range distortion components extend further than 13 Å from the vacant site. The displacements of surrounding atoms are strongly asymmetric with respect to the vacancy, contrary to previous theoretical results. We predict a strong relaxation in the lowest triplet excited state of the vacancy and small (less than 1 eV) triplet luminescence energy. The strong dependence of the defect properties on the radius of the relaxed region is demonstrated and the applicability of small molecular cluster models is discussed.

DOI: 10.1103/PhysRevB.66.024108 PACS number(s): 61.72.Bb, 61.72.Ji, 71.15.Dx, 42.70.Ce

I. INTRODUCTION

Silicon dioxide is an exceptionally important and versatile dielectric. It forms the passivating layer in metal oxide semiconductor technologies, it is the basis of most optical fibers, and its crystalline form, α-quartz, is important in oscillator technologies. In all of these applications, the nature and number of point defects is crucial to the reliability. As a consequence, the fundamental defects in both crystalline and a-SiO_2 have been studied intensely for the last 40 years. By far the most important defect is the oxygen vacancy. The vacancy has been implicated as the fundamental positive charge trap in bulk and thin-film a-SiO_2. It has also been considered as a model for one of the so-called oxygen-deficient centers (ODC's) in silica[1,2] that play an important role in the UV-induced refractive index changes in silica-based optical fibers (see, for example, Refs. 2–7). The experimental evidence reviewed in Refs. 1 and 8 suggest that it is a good candidate for a defect responsible for the 7.6 eV absorption band.

While there is much agreement about the qualitative nature of the oxygen vacancy, quantitative aspects of its structure in all charge states are not universally excepted.[1,8] One difficulty is that there is no universal method for calculation of defect properties. Both density-functional theory with periodic boundary conditions and finite molecular cluster calculations, which have been widely used to study defects in silica, have their own limitations. In the next section we briefly review the existing theoretical calculations and demonstrate that in all of them the defect-induced lattice deformation is confined to a very small region and does not include the full extent of the lattice perturbation by a defect. Full lattice relaxation can be accounted for in the embedded-cluster method, which treats a defect in an *infinite* polarizable lattice.

To address some of the deficiencies in existing theoretical methods, we have developed a hybrid technique[9–11] in which a quantum-mechanical atomic cluster is embedded in a classical atomistic representation of the solid. Details of the method are given below. As an application of this method to defects in ionic-covalent materials we have studied the neutral oxygen vacancy in quartz. The main result of this work is that the crystal deformation in the defect ground and first excited states exhibit strong anisotropy with significant displacements of the crystal ions within about 13 Å from the center of the vacancy. This result alters our understanding of the model of this defect, which has been viewed as a Si-Si bond formed due to symmetric displacements of two Si ions from their perfect lattice sites. Our results clearly demonstrate that the extent of the lattice deformation accounted for in the calculations can strongly affect other defect properties. Detailed analysis of the dependence of optical excitation and luminescence energies and defect formation energies on the extent of the lattice relaxation and on various parameters of the embedded-cluster model and the basis set shows strong limitations of the existing methods in terms of their ability to make reliable predictions of formation energies and optical-absorption spectra of ODC's in α-quartz. Strong relaxation of the excited state leads to a very small luminescence energy, suggesting that nonradiative transition may be much more effective. Although the atomic displacements in this diamagnetic defect cannot be compared directly with experimental data, we believe that the effect of long-range crystal deformation is general for other defects in silica, including E' and peroxy centers, and can be relevant to photoinduced densification of amorphous silica.

The balance of the paper is organized as follows. In Sec. II we review previous theoretical calculations to put the current work in context, and to demonstrate the unsettled state of the problem. In Sec. III we present a discussion of the embedding method. In Sec. IV we give our results, and conclude in Sec. V.

II. PREVIOUS THEORY

The neutral oxygen vacancy in silica is a diamagnetic defect and is usually characterized theoretically in terms of its geometric structure, formation energy, optical properties,

and its relation to the E' center. All existing calculations of the neutral oxygen vacancy in α-quartz predict a significant displacement of the two Si atoms neighboring the vacancy to one another, and the formation of a chemical bond between them. The equilibrium distance between these atoms predicted in most *ab initio* and semiempirical modified neglect of differential overlap (MNDO) cluster calculations[12–19] is in the range of 2.3–2.5 Å. The dependence of this parameter on the cluster size has recently been studied in Ref. 20 using the mechanical embedding method ONIOM. A larger Si-Si distance of 2.68 Å has been obtained by the quantum embedded-cluster method.[21] Periodic density-functional theory (DFT) plane-wave calculations reported in Refs. 22 and 23 predict 2.5 Å and about 2.7 Å, correspondingly. The periodic DFT calculations using gradient corrections and the projector augmented wave method[24] predict 2.44 Å. The Si-Si distance at the vacancy site is similar to the Si-Si spacing in elemental Si (2.35 Å) and much shorter than the equilibrium distance of 3.08 Å between the two Si atoms in ideal α-quartz. This is in marked contrast with cubic oxides, such as MgO,[13,25] and the more complex ZrO_2,[26,27] where, despite the substantial ionic polarization, the formation of a neutral oxygen vacancy leads to only very small displacements of the surrounding metal atoms. It is interesting to note that there is almost no discussion in the literature of the relaxation of the atoms surrounding the neutral vacancy. The relaxation of surrounding atoms proved to be vital for existence of the second, puckered configuration of the positively charged oxygen vacancy (see Refs. 19 and 23 and references therein). As we will show below, the extent and character of this relaxation strongly alters the existing model of the neutral vacancy and affects the calculated defect properties.

Optical absorption energy is crucial for experimental identification of this diamagnetic defect. In early calculations using non-self-consistent tight-binding methods (see references in Ref. 17), and in later, more rigorous semiempirical MNDO studies,[16–18] the absorption and luminescence bands of the neutral vacancy were related to the one-electron transition between the two states in the forbidden gap formed mainly by the bonding and antibonding combinations of the *sp* orbitals of the two silicon atoms adjacent to the vacant site. The energy of the lowest singlet-to-singlet excitation calculated by the MNDO method[16–18] was 5.0 eV. Further *ab initio* calculations in isolated clusters by Stefanov and Raghavachari[12] did not confirm these results. Instead, it was suggested that the lowest excitation has a much higher energy of ~7 eV and corresponds to a transition of different character: from the Si-Si bonding orbital to a diffuse state (i.e., a Rydberg-type excitation, not the bonding $\rightarrow$antibonding transition between strongly localized orbitals). On the other hand, the cluster calculations by Pacchioni *et al.*,[13–15] which also included diffuse atomic orbitals, confirmed the bonding-antibonding nature of the lowest one-electron allowed transition between the two vacancy levels in the gap. The energy of this transition was also 7–8 eV, similar to the result of Stefanov and Raghavachari,[12] and much higher than estimated with the semiempirical MNDO method in Refs. 16–18. Recent *ab initio* calculations of the oxygen vacancy in β-cristobalite, using the quantum embedded-cluster method implemented in the computer code EMBED,[21] again suggested the bonding$\rightarrow$antibonding transition model for the lowest vacancy excitation proposed earlier. The value of 8.3 eV for the lowest singlet-to-singlet excitation energy calculated in Ref. 21 corresponds better to the *ab initio* results obtained in Refs. 13–15 with the isolated cluster approach. Overall, according to *ab initio* calculations, the neutral oxygen vacancy is a good candidate for the ODC(I) center with the absorption band at 7.6 eV.[1]

Calculations also give the vacancy formation energy, with respect to the free oxygen atom in its lowest triplet state. As for the optical energies, previous predictions vary significantly. *Ab initio* calculations using the isolated cluster model give estimates of 5.5 and 6.7 eV at the Hartree-Fock (HF) level without and with *d* functions, respectively. The electron correlation correction calculated at the MP2 level for the basis set containing *d* functions brings the vacancy formation energy to 8.5 eV.[12,13] Quantum embedded-cluster calculations at the Hartree-Fock level[21] give about 6.6 eV for the vacancy formation energy in α-quartz and about 7.9 eV in β-cristobalite, respectively. The plane-wave density-functional theory (DFT) calculations in a periodic model give 6.97 eV in α-quartz[28] (with respect to the half of the energy of the oxygen molecule). Other DFT plane-wave calculations have given larger values of 7.85 eV (Ref. 29) and 8.64 eV (Ref. 30) for α-quartz, and 9.3 eV (Ref. 31) and 8.92 eV (Ref. 30) for β-cristobalite. Thus most of the *ab initio* results lie between 6.5 and 9.5 eV. The proposed thermodynamic estimate[32] of the vacancy formation energy is larger than 7.3 eV.

The calculations described above employ different quantum-mechanical methods (Hartree-Fock and DFT) and basis sets (atomic orbitals and plane waves) as well as different crystal models (periodic, isolated cluster, and embedded cluster). Therefore the apparent discrepancies in the calculated values are not easy to rationalize. However, they all suffer from the same problem—the defect-induced relaxation of the surrounding lattice is confined to a fairly small region around the defect. In the periodic calculations[23,28–31] the relaxation is limited by the size of periodic cell, which did not exceed 72 atoms. In the isolated cluster model,[12–15] clusters are much smaller and the dangling bonds of the atoms at the cluster border are saturated by Hydrogen atoms.[33] These calculations do not take into account the Madelung potential of the infinite lattice and neglect the lattice relaxation outside the cluster. The embedded-cluster calculations by the EMBED program[16,21] take into account the Madelung potential, but, due to time-consuming calculations, practically do not include the long-range lattice relaxation. Thus the full extent of the lattice relaxation caused even by one of the simplest intrinsic defects in quartz—neutral oxygen vacancy—is unknown. As will be shown below, the atomic displacements strongly affect all calculated defect properties. In particular, the lattice relaxation usually taken into account in previous calculations provides only about 50% of the total relaxation energy.

III. DETAILS OF CALCULATIONS

The embedded-cluster technique developed in our group and implemented in the GUESS computer code[9–11,34] allows

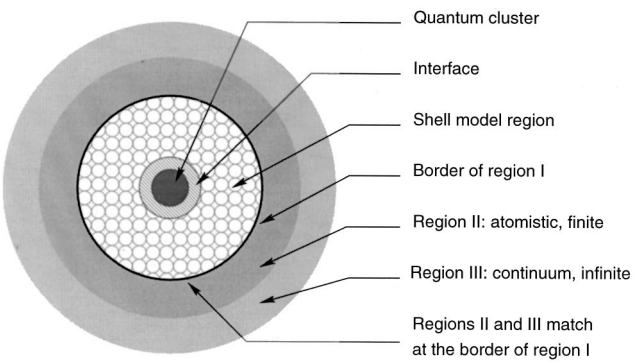

FIG. 1. General setup for the embeded-cluster calculations. See text for sizes of each region.

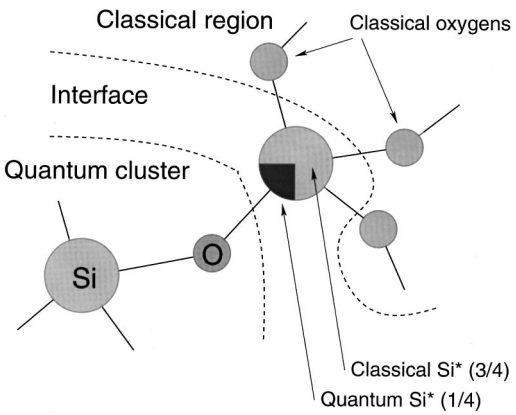

FIG. 2. Model for the interface between quantum cluster and classical environment. The boundary Si* is split into quantum-mechanical and classical parts. See text for details.

us to study point defects in crystals and amorphous solids combining quantum-mechanical treatment of atoms surrounding a defect with the shell model[35] representation of the rest of the solid. The main difference of this technique from the mechanical embedding ONIOM method employed in Ref. 20 is that it provides the consistent Madelung potential at the site of interest and allows one to account for both ionic and electronic contributions to the polarization of the defect environment.

In this approach, the infinite system with a single point defect is divided into several regions, as shown in Fig. 1. A spherical region I includes: (i) a quantum cluster with a defect and surrounding atoms treated quantum mechanically; (ii) an interface region, which connects the quantum cluster with the rest of the solid treated classically; (iii) a classical region, which includes up to several hundred atoms. Region I is surrounded by a finite region II, which is treated atomistically, and region III, which is treated in the approximation of polarizable continuum. Region III conforms geometrically to the boundary between regions I and II but extends to infinity (see Fig. 1). The classical ions in regions I and II are treated in the shell model[35] and interact between themselves via interatomic potentials.[36] Both quantum and classical atoms in region I are allowed to relax in the course of calculations. Atoms in region II are kept fixed in their ideal, bulk positions and provide correct variations of the electrostatic potential inside region I. Region III is used to calculate the polarization energy of the infinite lattice due to the presence of a defect in region I using the Mott-Littleton approach. Our setup is very similar to the original Mott-Littleton method of calculating point defects in polar solids.[37] It has then been refined in GULP,[38] and similar atomistic codes, as well as in the ICECAP embedding scheme.[39,40] The original computation scheme implemented in GUESS and applied to defect studies in ionic crystals has been described in Refs. 10, 11, 34, and 41. One of its main advantages is that it allows us to calculate forces on quantum-mechanical and classical ions and simultaneously optimize their positions using an effective energy minimization scheme.

In this work, we modify this scheme and apply it to an ionic-covalent system, α-quartz, which has directed bonds. Such systems present a challenge for cluster calculations due to the dangling bonds formed at the cluster border. The electronic states associated with these bonds strongly perturb the cluster electronic structure and make it a poor mimic of an infinite system. Therefore in most cases these bonds are saturated by real or pseudohydrogen atoms. This method is discussed in detail in Ref. 33. Our approach is different in that it embeds a quantum-mechanical (QM) cluster into a continuous crystal instead of treating it as a molecule. Therefore the interface atoms play a special role in this procedure as described below.

All QM clusters in our calculations are terminated by Si atoms, with one neighboring O atom always belonging to the QM cluster and with the other three neighboring O atoms belonging to the classical environment. These terminating (interface) Si species are called pseudo-Si atoms (Si*) and perform dual functions, as illustrated in Fig. 2.

The first function of Si* atoms is to describe a Si-O bond directed inside the QM cluster (see Fig. 2). For the electrons and cores inside the QM cluster they look like a one-electron atom with the effective charge equal to that on a regular lattice Si atom and an *sp* orbital centered on it. Since effective charges on Si atoms in quartz are about $+2.4\,|e|$ (e is the electron charge) it represents a strong attractive center for cluster electrons. To compensate locally the resulting strong electrostatic potential, an effective repulsive electronic potential $V(r)=A\times\exp(-\mathrm{Br})$ is added to mimic a screening of the Si core potential by valence electrons. The parameters of this potential and of the basis set for the Si* atoms were optimized to satisfy the following conditions. (i) The electronic charge is evenly distributed within the QM cluster or, in other words, the effective charge modulus on Si* is approximately equal to $\frac{1}{4}$ of that on regular quantum Si atoms and $\frac{1}{2}$ of that on quantum O atoms. (ii) The electronic states associated with Si* atoms do not have substantial contributions at the top of the valence band or at the bottom of the conduction band. The short-range interaction between the boundary Si* atoms and their nearest oxygen neighbors in the QM cluster is modelled using a Morse-type classical potential, which ensures a good approximation of the interatomic distance between the two species.

The second function of Si* atoms is to interact with the shell-model ions outside the QM cluster. This interaction has Coulomb and short-range components. The interaction of

point charges representing cores and shells of classical ions in regions I and II with the electron on the *sp* orbital of Si* is included in the Fock matrix via the matrix elements of the same type as the electron-nuclei interaction. In addition, these ions interact classically with the $\frac{3}{4}$ of the effective charge of the classical Si ion also centered on Si*. Thus Si* might be envisaged as comprising $\frac{1}{4}$ from quantum parts and $\frac{3}{4}$ from classical parts (see Fig. 2). Note that the effective charge of Si* can vary, as it depends on the population of its *sp* orbitals. The short-range terms are described by interatomic potentials.[36] These originally rigid ion potentials were modified by including shells on oxygen ions. They are also used in order to describe the interactions between the classical atoms in region I and between the classical and quantum atom. The latter are introduced in order to mimic the exchange and resonance component of the interaction between the classical and quantum atoms across the QM cluster boundary. The expression for the total energy of the system is given in the Appendix.

The electrostatic potential produced by classical ions in regions I and II depends on their effective charges, which are parameters of interatomic potentials. The potentials[36] used in this work have been fitted using fractional ionic charges ($Q_{\mathrm{Si}}=2.4\,|e|, Q_O=-1.2|e|$) to reproduce accurately several of the SiO_2 polymorphs. These ionic charges have been obtained from *ab initio* calculations of small clusters using the 6−31G* basis set.[36] As is shown below, these charges are fairly close to those obtained in our embedded-cluster calculations using natural population analysis (NPA).[42] The latter depend, however, on a basis set. In a fully consistent approach, the charges on ions in QM clusters and those on classical ions in the perfect lattice should be the same. In the present work we tried many different basis sets and this condition is not fully satisfied for all of them. Nevertheless we believe that this does not affect our qualitative conclusions regarding the extent and character of the lattice relaxation around the defect.

Region I+II may have different shapes and should be neutral and have zero total dipole moment. To build this region we used $Si(O_{1/2})_4$ units, which provide convenient stoichiometric elements with a very small (often practically zero) dipole moment. With this choice, a spherical region I +II gives the fastest convergence for the electrostatic potential. In our present calculations, region I+II has radius 30 Å and contains 9270 atoms. The finite size of the system results in a spread of the electrostatic potential at atomic sites, which should be equivalent in the infinite crystal. For the region I+II used in this work, the spread of the potential within region I was less than 0.01 eV, which indicates that the system was large enough to mimic the electrostatic potential in the infinite crystal. In most calculations discussed below region I had a radius of 13.07 Å and contained 718 atoms.

Because region II remains fixed, its geometric structure can affect the positions of atoms in region I and in the QM cluster when they have been allowed to relax in defect calculations. In building region I+II one has a choice of the experimental structure or those determined in shell-model and quantum-mechanical calculations of the perfect system in the periodic model. These structures differ slightly and we checked the effects of these differences on defect properties. For that purpose we optimized the geometry of α-quartz using the GULP code[38] and the pair potentials.[36] Then the region I+II was built using these geometric parameters and the vacancy structure and its formation energy were calculated. The same procedure was repeated using the best α-quartz structure found in the Hartree-Fock CRYSTAL calculations.[43] The thus calculated formation energies differ by less than 0.03 eV. The shell-model ions in perfect α-quartz are polarized, i.e., positions of ionic shells differ from positions of cores, which results in a small dipole being associated with each ion. We have also checked that far from the vacancy these small dipoles do not affect the results of defect calculations and one can treat region II in a point-ion model.

The GUESS code provides an effective interface between the quantum-mechanical treatment of QM clusters using the GAUSSIAN98 code[44] and the classical treatment of the rest of the system. The electronic structure of QM clusters was calculated using the unrestricted Hartree-Fock (UHF) method and different standard basis sets ranging from 3–21G to 6–311G* for both silicon and oxygen atoms. QM clusters of different sizes and topology have been considered: $Si_2O_7Si_6^*$ (cluster 1), $Si_8O_{25}Si_{18}^*$ (cluster 2), $Si_{10}O_{30}Si_{20}^*$ (cluster 3), and $Si_{18}O_{49}Si_{26}^*$ (cluster 4) with the oxygen atom in the center (see Fig. 3). Note that all these clusters are stoichiometric, i.e., the ratio of the numbers of oxygen and silicon atoms (Si* being the quantum-mechanically treated $\frac{1}{4}$ of a silicon atom, as discussed above) is equal to 2. Indeed, each boundary Si* atom is treated as a $Si_{1/4}$ species and therefore each cluster can be viewed as built from $Si_{1/4}O_{1/2}$ bondlike elements, which are stoichiometric. When increasing the cluster size we aimed to satisfy the additional criterion that the cluster must be compact. The compactness of a given cluster can be defined as the ratio $\eta=N_{\mathrm{cluster}}/N_{\mathrm{crystal}}$, where N_{cluster} is the sum of quantum-mechanically treated nearest neighbors for each atom in the cluster and N_{crystal} is the sum of all nearest neighbors of the cluster atoms in the crystal. For the infinitely large cluster $\eta=1$; for the clusters used in the present study, η increases from 0.58 for cluster 1 to 0.72 for cluster 4.

To test our embedding scheme we carried out so-called ''perfect lattice test'' calculations for each cluster. In these calculations a nondefective QM cluster was embedded in the rest of the lattice and the whole system was allowed to relax. In the case of ''ideal'' embedding, no atoms in region I should displace from their original sites. In practice, we observed a relatively small relaxation associated with the interface region, where the maximum displacements of atoms, changes in the interatomic distances, and changes of the ''soft'' Si-O-Si angles with respect to their original values were less than 0.15 Å, 4%, and 5% respectively. Distortions in the rest of the system were at least three times smaller. We also checked that after relaxation the electronic structure of the cluster did not undergo any noticeable modification, i.e., there was no change in electron-density distribution within the QM cluster or in the density of states.

When a neutral vacancy ≡Si—Si≡ is created by removing the central oxygen atom in one of the QM clusters men-

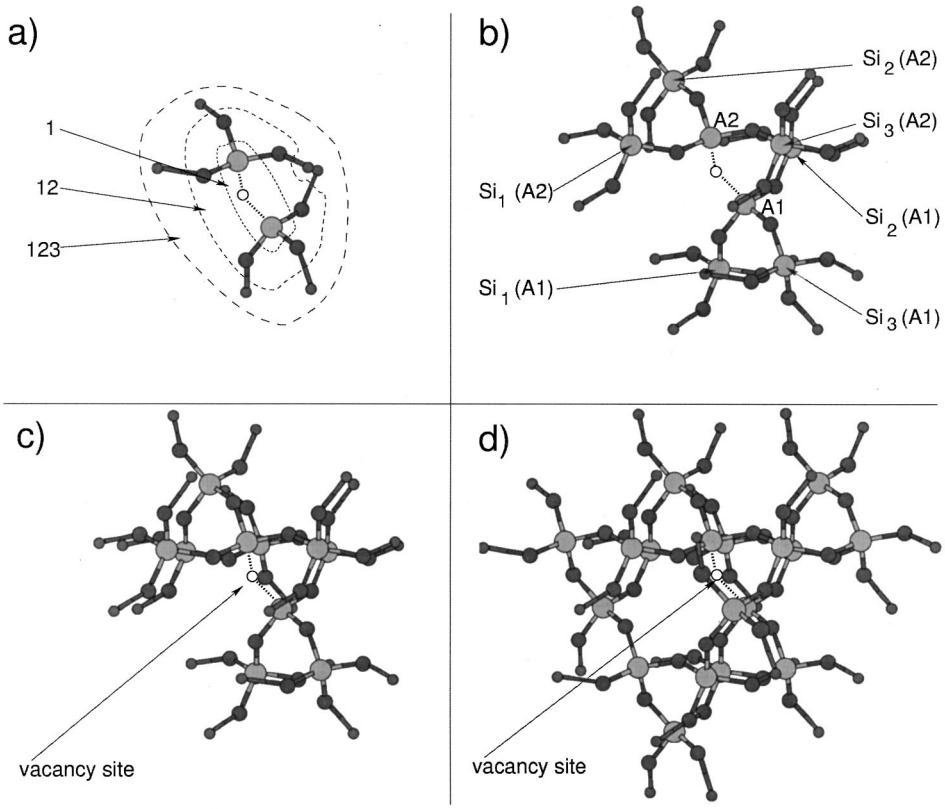

FIG. 3. Quantum clusters (including Si* atoms) used in the calculations shown in the same projection. (a) cluster 1; (b) cluster 2; (c) cluster 3; (d) cluster 4. Additionally, (a) shows atoms included into partial relaxation near the vacancy (see also Table I); (b) shows Si atoms A1 and A2 and their nearest Si atoms, which are labeled Si_1, Si_2, Si_3 (see discussion in the text).

tioned above (Fig. 3), the formation energy is calculated as

$$E_{\text{for}} = E_{\text{tot}}(V) + E(O) - E_{\text{tot}}(\text{perfect}), \tag{1}$$

where $E_{\text{tot}}(V)$ and $E_{\text{tot}}(\text{perfect})$ are the total energies of the system with the vacant site and the perfect system, respectively, and $E(O)$ is the UHF energy of the free oxygen atom in the ground triplet state. To model oxygen vacancies associated with substitutional Ge atoms [Ge ODCs (Ref. 45)], we considered oxygen vacancies with one or two neighboring silicon atoms substituted by germanium atoms (i.e., vacancies ≡Si—Ge≡ and ≡Ge—Ge≡). Their formation energies were calculated using a definition analogous to Eq. (1). However, in these cases, the perfect system contains one or two germanium atoms (≡Si—O—Ge≡ and ≡Ge—O—Ge≡).

Unless otherwise stated, all calculations included a counterpoise correction for the basis set superposition error (BSSE) (Ref. 46) (see also recent discussion in Ref. 47). This means that the oxygen basis set remained centered in the vacancy when an oxygen atom was removed to form a vacancy. Similarly, the oxygen atom energy was calculated including the basis sets of all other atoms in each particular QM cluster centered at the positions of these atoms around the vacancy.

We used several methods for calculating the optical excitation and luminescence energies in the Franck-Condon approximation. Calculations were performed for the defect geometries corresponding to the fully relaxed S_0 state ($S_0^* \rightarrow T_1$ in our tables) and T_1 state ($T_1^* \rightarrow S_0$). In these notations (*) means a fully relaxed state. The excitation energies from the ground singlet state S_0 to the lowest triplet state T_1 and the luminescence energies from the relaxed triplet state were calculated taking the differences between the total energies of the system in the triplet and singlet states (ΔSCF). To pinpoint excitations associated specifically with the bonding and antibonding orbitals of the vacancy site (e.g., $S_0^* \rightarrow S_1$, $S_0^* \rightarrow T_1$ in our tables) and estimate oscillator strength of dipole electronic transitions we used a configuration interaction technique which takes into account single-electron excitations (CIS),[48] as implemented in the GAUSSIAN98 code.[44] Finally, more accurate calculations for luminescence energies were carried out using a coupled cluster method with double excitations (CCSD).[49]

IV. STRUCTURE AND PROPERTIES OF ANION VACANCY

A. Defect structure in the ground state

In Sec. II we observed that, whereas previous calculations predicted similar structures for the neutral oxygen vacancy in α-quartz, the energies predicted depended on particular details of the method used. In our embedded-cluster approach, we find that the quantitative results also depend on the basis set and, to a smaller extent, on the shape and size of the QM cluster. We shall analyze this dependence in more detail below. In this section we will focus on the effects of the lattice relaxation on defect structure and properties. The full extent of this relaxation can be established only from an embedded-cluster technique such as that employed in this work, or from a solid-state calculation with a very large supercell. The main

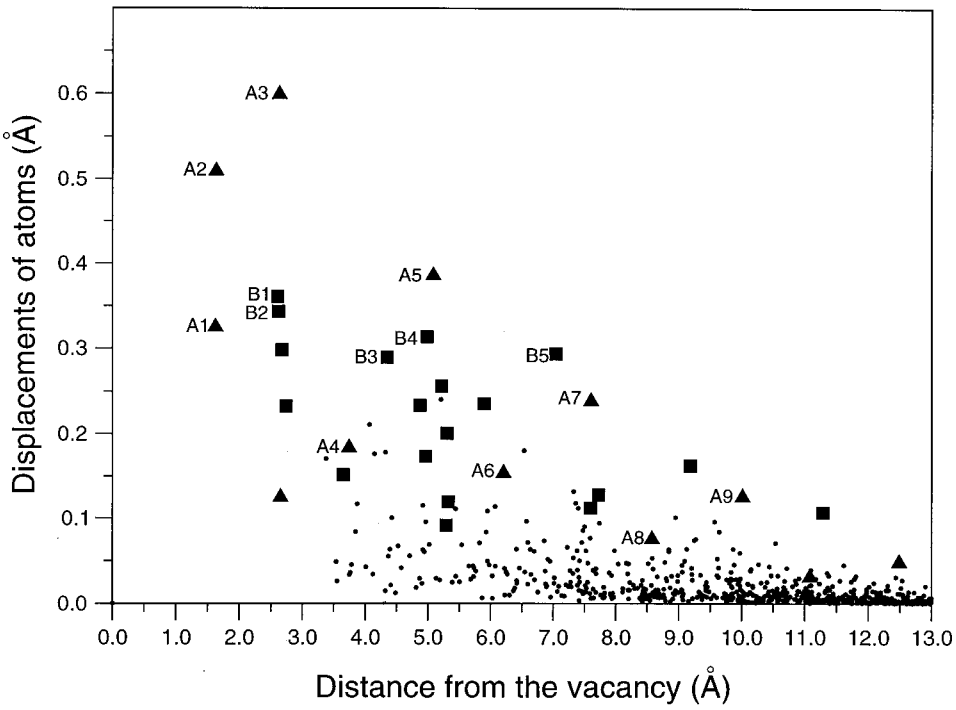

FIG. 4. Total displacements of atoms resulting from the relaxation near the vacancy. Atoms participating in the relaxation of A and B types are shown as triangles and squares, respectively. Numbering of the atoms corresponds to that in Figs. 3(b), 5, and 6.

results can be clearly seen in the calculations of two smaller clusters 1 and 2 [Figs. 3(a) and (b)] in the 6−31G basis set.

The results of these calculations suggest that the rest of the lattice allows the Si atoms to relax without serious inhibition, driven by bond formation. Nevertheless, their strong displacement induces a complicated distortion of the whole region I. The atomic displacements decrease for distant atoms, but the number of these atoms increases rapidly and the resulting effect on defect properties is not negligible. The absolute values of atomic displacements from the nondefective lattice sites as a function of their distance from the vacant oxygen site are presented in Fig. 4. One can clearly see that displacements decrease to almost zero values (0.01 Å) only at the outer boundary of region I (13.07 Å). They are still about 0.2–0.4 Å at 5 Å from the vacant site (the sixth neighboring shell) and are not negligible even at 10.0 Å from the vacancy. We have analyzed whether the noted decrease in atomic displacements with the distance from the defect center R could be described by an R^{-2} dependence, which one could expect from a continuum model. However, it turned out that the defect-induced displacement field is more complicated and cannot be easily fitted by this simple function.

Further analysis of the character of atomic displacements demonstrates that they can be clearly divided into two types, shown in Figs. 4 and 5(a) and (b). Type A is extremely anisotropic due to the absence of the center of inversion in quartz. It involves large displacements of the silicon and oxygen atoms directed towards the vacancy approximately along the line connecting the two Si atoms neighboring the vacancy. The displacements of the silicon atoms, A1, A2, A4, A6, A8 are smaller and die much more rapidly than those of the oxygen atoms marked as A3, A5, A7, A9 in Figs. 4 and 5(a).

Atomic displacements of the second type, marked B in Figs. 4 and 5(b), are more isotropic and correspond predominantly to the relaxation of Si-O-Si angles. This peculiar relaxation demonstrates high flexibility of the quartz structure. It is long range and far exceeds the size of any molecular cluster or periodic cell used in previous calculations. Displacements of Si atoms are much smaller than displacements of oxygens. For example, there are only two Si atoms (those near the vacancy site) in the whole region I, which relax by more than 0.2 Å, while there are 16 such O atoms.

We may check whether the size of region I is sufficient for describing such a strong long-range relaxation by increasing its radius to 15.03 Å, which corresponds to including altogether 1120 atoms. This had a very small effect on the distance between the silicon atoms adjacent to the vacant site (~0.01 Å) or on the vacancy formation energy (~0.03 eV). The additional displacements of atoms situated at a distances less than 13 Å from the vacancy are also very small. Atoms participating in relaxation of types A and B were additionally displaced by no more than 0.03 Å, while typical displacements were less than 0.01 Å. Thus we conclude that the lattice relaxation induced by neutral oxygen vacancy in α-quartz is highly anisotropic and has a radius of about 13.0 Å. The relaxation certainly will differ for different defect types (e.g., impurities, interstitials, etc.), but one could expect equally strong or even larger relaxation for the excited state of the neutral vacancy and for the vacancy in different charge states.

The two neighboring Si atoms which bond on forming the neutral oxygen vacancy are not equivalent in the perfect α-quartz structure due to the absence of the center of inversion. Once the vacancy has been formed these Si atoms therefore have *different* displacements near the vacancy. As can be seen in Fig. 4, one of the Si atoms (A2) is displaced by about 0.5 Å and the other (A1) only by about 0.3 Å from the nondefective lattice sites. The α-quartz structure can be viewed as a network of corner-sharing tetrahedra where the

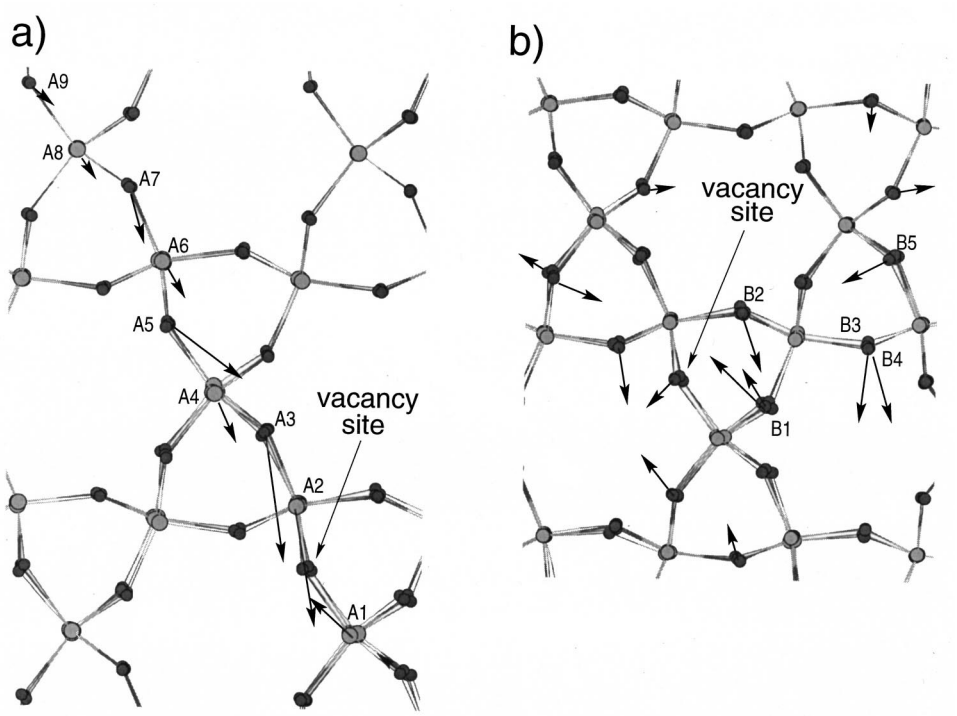

FIG. 5. Projections of directions of atomic displacements near the vacancy. The length of each arrow corresponds to the magnitude of actual displacement multiplied by a factor of 4 for better visibility. Note that atoms are shown in their positions in the nondefective lattice. Notations and numbering correspond to those in Figs. 3(b), 4, and 6.

two Si atoms near the vacancy site are each at the center of a corresponding tetrahedron [Fig. 3(b)]. The effect of this structure on the relaxation of the Si atoms, A1 and A2, can be understood analyzing the geometry of the Si sublattice. The difference in A1-A2-Si_k(A2) and Si_k(A1)-A1-A2 angles with surrounding three Si atoms [where $k=1,2,3$; see Fig. 3(b)] is a measure of the difference in the arrangement of the tetrahedral units in the vicinity of the vacancy site. For the perfect structure the A1-A2-Si_k(A2) angles are 139°, 107°, and 91°, while the Si_k(A1)-A1-A2 angles are 123°, 108°, and 90°. The values of the first angle are significantly different and determine the magnitude of relaxation. The asymmetric arrangement of neighbors around an oxygen vacancy has first been discussed in slightly different terms than used here by Griscom and Cook[50] and by Rudra and Fowler.[51]

We have estimated that the dipole moment of the relaxed vacancy in the both ground and excited triplet electronic states is equal to about 1.9 D and is directed approximately perpendicularly to the line connecting the two Si atoms A1 and A2. This can be qualitatively explained if we note that each of the elementary structural units $Si_{1/4}$-O-$Si_{1/4}$ of the quartz structure also has a dipole moment of the same order oriented in opposite direction. The total dipole of the ideal crystal is equal to zero due to cancellation of the above dipole moments. However, creation of the vacancy and its asymmetry results in an uncompensated dipole moment, which is a collective effect of the whole distorted lattice. We should note that the electron density is distributed almost equivalently between the Si atoms A1 and A2 and therefore their contribution to the dipole moment of the vacancy is insignificant.

B. Effect of lattice relaxation on defect properties

It is instructive to see how the defect properties depend on the extent of the lattice deformation accounted for in the calculations. In Table I we present the main characteristics of the vacancy as a function of the number of neighboring atoms, which were allowed to relax. Notations 0, 1, 12, 123, and ''full'' have the following meanings [see Fig. 3(a)]: 0: no atoms were relaxed; 1: two silicon atoms neighboring the vacancy relaxed; 12: as in 1 with a further six oxygen atoms relaxed; 123: as in 12 with a further six Si atoms relaxed; ''full:'' relaxation of all species in region I (including shells on the classical atoms). For comparison, a commonly used molecular cluster $Si_2O_6H_6$ with fixed border H atoms would correspond to the relaxation type ''12'' in this notation. As one can see, the equilibrium Si-Si distance changes by about 0.8 Å dependent on the number of degrees of freedom involved in geometry optimization. With full relaxation, the equilibrium distance between the two Si atoms is equal to 2.36 Å, essentially identical to the Si-Si spacing in elemental silicon. These values remain practically the same for larger clusters calculated in the same, 6–31G, basis set.

The number of quantum and classical atoms included in the relaxation has a dramatic effect on the vacancy formation energy. The values presented in Table I in rows marked 0–123 (calculated with respect to the free oxygen atom in its ground triplet state) do not include the BSSE correction. They demonstrate that the vacancy formation energy decreases by about 2 eV as increasing number of O and Si neighbors are allowed to relax. Inclusion in the relaxation of the more distant atoms from the fourth and further neighboring shells results in the further energy decrease of about 0.75–0.93 eV (Table I), which is more than a third of the total energy gain during the relaxation. The value for the vacancy formation energy, calculated with the BSSE correction, is found to be about 3.6 eV (see Table I) for both clusters 1 and 2 in 6–31G basis set.

A qualitatively similar dependence of the defect properties on the number of surrounding atoms accounted for in the

TABLE I. Properties of the neutral oxygen vacancy calculated using $Si_2O_7Si_6^*$ and $Si_8O_{25}Si_{18}^*$ clusters in the 6–31G basis set. Notations 0–123 represent different types of relaxation accounted for in calculations (see text for details). E_{for} is the formation energy of the relaxed vacancy in the ground singlet S_0^* state. The asterisk (for example, S_0^*) means that the equilibrium geometry of the respective state has been used. R_S and R_T are the equilibrium distances between the two central Si (or Ge) atoms for the S_0^* and T_1^* states, respectively. $\varepsilon_b - E_v$ is the difference between the one-electron energy level of the vacancy ε_b and the level representing the top of the valence band E_v. The values in the $S_0^* \rightarrow S_1$ column are the absorption energies (left) and oscillator strengths *f*, calculated using CIS. Energies of the $S_0^* \rightarrow T_1$ and $T_1^* \rightarrow S_0$ transitions are also calculated using the CIS method. The values of $T_1^* \rightarrow S_0$ luminescence energies given in brackets in the last column are calculated by the CCSD method. "BSSE" marks the properties calculated including the BSSE correction. All energies are in eV and distances in Å.

Cluster type	Relaxation type	E_{for}	R_S	$\varepsilon_b - E_v$	$S_0^* \rightarrow T_1$	$S_0^* \rightarrow S_1$		R_T	$T_1^* \rightarrow S_0$
$Si_2O_7Si_6^*$						*E*, eV	*f*		
	0 (no relaxat.)	6.88	3.13	5.08	1.26	5.26	≈1	3.13	1.26
	1 (relax 2Si)	6.56	2.86	3.11	2.65	6.16	≈1	3.20	0.91
	12 (relax 1+6O)	6.09	2.70	2.63	3.55	6.57	0.82	3.18	0.91
(embedded)	123 (relax 12+6Si)	5.62	2.52	2.11	4.96	7.18	0.48	3.28	0.41
	full (relax region I)	4.84	2.36	1.96	6.01	7.58	0.25	3.36	−0.32 (0.49)
	full+BSSE	3.58	2.32	1.67	6.13	7.52	0.13	3.21	0.28 (1.05)
	Si-Ge, full	4.27	2.38	1.62	6.00	7.55	0.27	3.34	−0.34 (0.47)
	Si-Ge, full+BSSE	3.01	2.35	1.29	6.12	7.50	0.12	3.19	0.35 (1.07)
	Ge-Ge, full	3.73	2.40	1.81	5.95	7.51	0.30	3.41	−0.59 (0.22)
$Si_2O_7Si_6^*$	fixed H	5.76	2.61						
(isolated)	relaxed H	4.58	2.32						
$Si_8O_{25}Si_{18}^*$	Si-Si, full	4.55	2.35	1.92					
(embedded)	Si-Si, full+BSSE	3.55	2.32	1.68					
	Si-Ge, full	3.92	2.38	1.73					

geometry relaxation has also been noted in Ref. 20. The results presented in Table I allow us to make a direct comparison with the results of other calculations using molecular clusters and similar basis sets. These can be divided roughly into two groups: (i) with fixed positions of saturating hydrogen atoms, and (ii) those where the saturating hydrogen atoms were also allowed to relax. The relaxation in the first group was in most cases restricted to the type "12" in Table I and the Si-Si distance obtained in these calculations is about 2.55 Å (see, for example, Refs. 13–15). Clusters in the second group correspond to full relaxation but are much "softer" due to the absence of constraints on displacements of boundary atoms. This leads to much shorter Si-Si distances, such as 2.32 Å obtained in Ref. 12.

For comparison, we performed similar calculations ourselves (see Table I). These calculations for a small cluster 1 and the 6–31G basis set demonstrated that the cluster with fixed H atoms gives much larger Si-Si distance and vacancy formation energy and that the cluster with relaxed H atoms correspondingly smaller values than obtained in our embedded-cluster calculations. The effect of restricted relaxation has also been observed in other calculations. For example, the Si-Si distance of 2.68 Å obtained with the EMBED method[21] is considerably larger than 2.36 Å reported here. This is because the atomic relaxation only included Si and O atoms nearest to the vacancy. It is interesting to note that the Si-Si distance found in periodic DFT calculations is also systematically longer than 2.4 Å,[22–24] which again reflects significant constraints on the lattice relaxation around a defect imposed by the size of the unit cell. Due to the same reason all previous calculations failed to find the asymmetry in the relaxation around the vacancy.

Table I also demonstrates the effect of the lattice relaxation on other defect properties calculated in clusters 1 and 2. In particular, the position of the double occupied level of the neutral vacancy with respect to the top of the valence band shifts markedly as more atoms are allowed to relax and stabilizes at about 1.7–2.0 eV when the full relaxation is included. This level has a bonding character with respect to the AO's of the two neighboring silicon atoms. In the small cluster 1 in the 6–31G basis set the first unoccupied state in the one-electron spectrum is also located in the band gap and has an antibonding character with some contributions of neighboring oxygen AO's.

The lowest singlet-to-triplet ($S_0^* \rightarrow T_1$) and singlet-to-singlet ($S_0^* \rightarrow S_1$) optical transitions calculated using the CIS method are dominated by the one-electron transitions between these two localized states. The calculated lowest $S_0^* \rightarrow S_1$ excitation energy for the fully relaxed vacancy (see Table I) is equal to 7.6 eV. This energy is close to one of the observed defect absorptions, but we believe that the agreement is likely to be coincidental. Note again the dramatic dependence of the excitation energies on the number of atoms included in the lattice relaxation seen in Table I.

C. Neutral vacancy in Ge-doped α-quartz

We have also performed calculations for the vacancy where one or two Si atoms were substituted by Ge. The

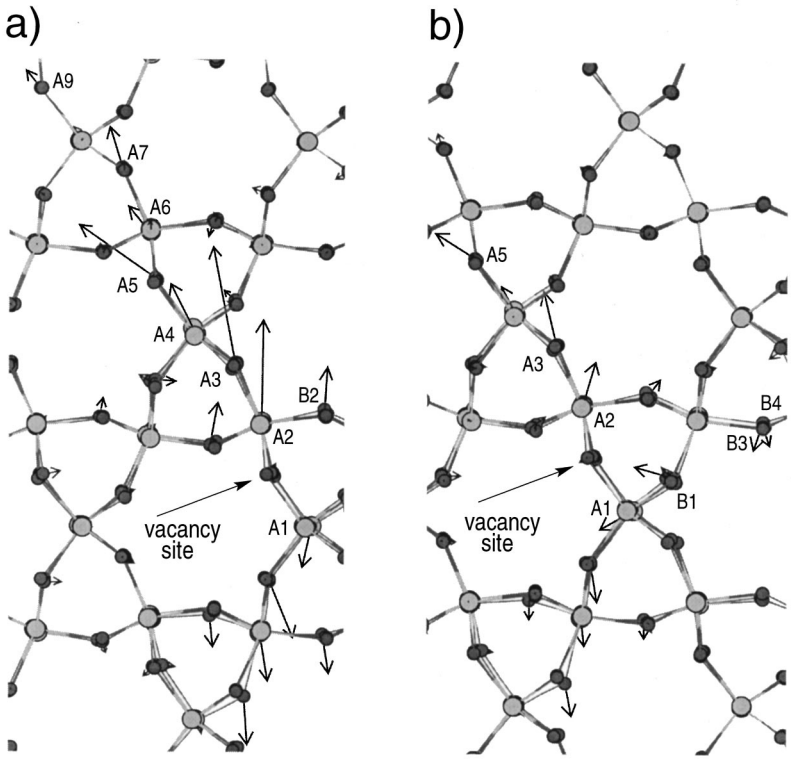

FIG. 6. (a) Displacements of atoms near the vacancy after the relaxation in the triplet excited state calculated with respect to the geometry of the vacancy ground state. (b) similar displacements calculated with respect to the geometry of the nondefective lattice. The length of each arrow corresponds to the magnitude of actual displacement multiplied by a factor of 4 for better visibility. Note that atoms are shown in their positions in the nondefective lattice. Notations and numbering correspond to those in Figs. 3(b), 4, and 5.

Si-Ge spacing (Si-Ge vacancy) is 2.38 Å, and the Ge-Ge spacing (Ge-Ge vacancy) 2.40 Å, very close to the Ge-Ge spacing of 2.45 Å in elemental Ge. Analysis of the character of the lattice relaxation demonstrates very similar features to those discussed above.

The formation energy of the vacancy with one or two neighboring silicon atoms substituted by a germanium atom is lower than that for the pure quartz because of the weaker Ge-O bond. This result is similar to that obtained in Ref. 18 using the semiempirical MNDO method. The lower formation energy may explain the well-known experimental fact that in Ge-doped silica *glass* only Ge ODC's are observed. Thus if ODC's are vacancies, then only ≡Si—Ge≡ and ≡Ge—Ge≡ defects are observed; there are no ≡Si—Si≡ defects. The following structural transformations are exothermic in Ge-doped silica:

$$\equiv\mathrm{Si}\text{—}\mathrm{Si}\equiv + \equiv\mathrm{Si}\text{—}\mathrm{O}\text{—}\mathrm{Ge}\equiv \rightarrow \equiv\mathrm{Si}\text{—}\mathrm{Ge}\equiv + \equiv\mathrm{Si}\text{—}\mathrm{O}\text{—}\mathrm{Si}\equiv + E_{R1},$$

$$\equiv\mathrm{Si}\text{—}\mathrm{Ge}\equiv + \equiv\mathrm{Si}\text{—}\mathrm{O}\text{—}\mathrm{Ge}\equiv \rightarrow \equiv\mathrm{Ge}\text{—}\mathrm{Ge}\equiv + \mathrm{Si}\text{—}\mathrm{O}\text{—}\mathrm{Si}\equiv + E_{R2}.$$

For both reactions, the calculated energy gain is almost the same: $E_{R1} \simeq E_{R2} \simeq 0.6$ eV, suggesting that formation of Ge ODC's is indeed energetically profitable. Electronic excitation, whether by an electron beam or by ultraviolet excitation, should stimulate these processes, since excitation causes oxygen motion.

D. Excited triplet state

As noted above, the triplet excited state is as poorly understood as the singlet one. The results presented in Table I (which are also confirmed using different clusters and basis sets) demonstrate that in spite of high excitation energy, the energy of the luminescence transition $T_1^* \rightarrow S_0$ is very small. This results from a strong relaxation in the excited triplet state which moves the Si (or Ge) atoms apart from the vacant site. This relaxation is due to the repulsion between the two Si atoms adjacent to the vacant site.[17] As one can see in Fig. 6, this repulsion drives the lattice relaxation back beyond the perfect lattice configuration; indeed, the distance between the two Si atoms A1 and A2 even exceeds that in the perfect lattice (Table I). However, the vacancy remains in the configuration where the vertexes of the two SiO_3 pyramids are pointing towards the vacant site (see Fig. 3).

As one can see in the last column of Table I, the luminescence energies calculated using the CIS method are negative when the oxygen basis set is not retained in the vacant site. The same tendency is observed in the ΔSCF calculations. However, more accurate calculations using the CCSD method give positive luminescence energies in all cases considered (see Table I). The relatively large $S_0^* \rightarrow T_1$ absorption energy and low $T_1^* \rightarrow S_0$ emission energy correspond to a large relaxation energy of 2.85 eV in the excited state. Both transitions will be relatively weak, since they are spin forbidden, and are allowed only when spin-orbit coupling is included. Therefore optical absorption will take place into the singlet state with further spin conversion. Ge has a much larger spin-orbit coupling than Si, so the Ge centers could be visible in triplet absorption. Further, the large relaxation energy in the triplet excited state implies a large Huang-Rhys

TABLE II. Parameters of the oxygen vacancy and of the perfect crystal calculated for the cluster $Si_2O_7Si_6^*$ using different basis sets. O_1 is the central oxygen ion in the cluster. The BSSE correction is a sum of the correction to the energy of the vacancy and that to the energy of the free oxygen atom in the ground (triplet) state. The latter can be quite large. It is about 0.5 eV for the 6–21G* basis set and exceeds 2.0 eV for the 3–21G basis set. Other notations are as in Table I.

Basis set		Vacancy				Perfect crystal				
Si	O	E_{for}^* eV	Si-Si Å	q_{Si} $\|e\|$	$\varepsilon_b - E_v$ eV	Si-O1 Å	Si-O-Si °	q_O $\|e\|$	q_{Si} $\|e\|$	BSSE corr. eV
3–21 G	3–21 G	4.65	2.21	1.95	1.23	1.62	147	−1.27	2.51	2.65
3–21 G*	3–21 G	5.63	2.31	1.96	2.03	1.60	146	−1.29	2.56	1.90
6–21 G	6–21 G	5.02	2.34	1.93	2.00	1.62	146	−1.26	2.51	1.81
6–21 G*	6–21 G	6.34	2.36	1.94	2.41	1.61	145	−1.28	2.54	0.46
6–21 G*	6–21 G*	6.63	2.38	1.89	2.35	1.61	142	−1.28	2.51	0.75
6–31 G	6–31 G	3.58	2.32	2.22	1.67	1.61	151	−1.33	2.82	1.26
6–31 G*	6–31 G*	6.08	2.37	2.12	2.17	1.59	147	−1.35	2.76	0.36
6–21 G*	6–31 G*	6.42	2.41	2.14	2.22	1.59	150	−1.35	2.79	0.44

[a]Basis set (Ref. 43).

factor and linewidth at zero temperature. However, the latter cannot be easily estimated from a simple theory[52] as the profile of the adiabatic potential of the T_1^* state is very different from that of the S_0^* state. The large relaxation energy E_R also indicates that the excited state should recover nonradiatively, since the ratio E_R/absorption energy is much bigger than $\frac{1}{4}$ (see Ref. 52).

Finally, we note that the results obtained in this basis set for a larger cluster 2 are very similar to those described above (see also Table I). More significant quantitative variations obtained for different basis sets are discussed in the next section.

V. EFFECT OF COMPUTATIONAL PARAMETERS

Cluster calculations in localized basis sets are inevitably a compromise between cluster size and basis set. The cluster size is generally determined by the strength of the defect-induced perturbation and one tries to use as wide a basis set as practical. However, there is always a question as to what extent the results are affected by these two factors. We tried to address some of these issues by systematically increasing the basis set for a relatively small cluster and then considering several clusters in selected basis sets.

A. Effect of basis set

The results calculated in cluster 1 for the perfect and defective systems for several basis sets are summarized in Table II. First, one can see that the characteristics of the perfect crystal are quite close for all basis sets. The Si-O distance in the quantum part of the cluster tends to decrease by about 0.01 Å for more extended basis sets including *d* orbitals, such as 6–31G*. Variations of the Si-O-Si angle presented in Table II are of the order of 5°. The effective atomic charges are almost the same for all the basis sets. The Si-Si distance in the relaxed vacancy also remains broadly the same for all the basis sets. Therefore the character of the lattice relaxation is qualitatively very similar to that discussed in the previous section. The creation of the vacancy results in a considerable increase of the electron density on the two silicon atoms adjacent to the vacant site and in the respective decrease of their effective charges as a result of elimination of the electronegative oxygen atom. However, these charges do not change significantly for extended basis sets (see Table II). We have also checked the basis set dependence of our results for an isolated $Si_2O_7H_6$ cluster where all atoms were allowed to relax. We considered basis sets from STO-3G to double zeta with polarization functions, with and without an oxygen basis at the center of the Si-Si bond. These results demonstrate essential convergence at the 6–31G level. The Si-Si distance increased by about 0.07 Å as the basis was extended from 3–21G to DZ+*d* level. These results are again in qualitative agreement with embedded-cluster calculations shown in Table II.

The vacancy formation energy, however, strongly depends on the basis set, and varies in the range of 3.6–6.6 eV. These strong variations are difficult to rationalize and we believe that they are partly due to narrow basis sets employed and partly due the QM cluster boundary effects. This is also reflected in the values of BSSE corrections shown in Table II. Inclusion of *d* orbitals reduces the variations in formation energies to 1 eV. The importance *d* orbitals on oxygen atoms for the correct description of different crystalline modifications of SiO_2 has been noted by Civalleri *et al.*[43] who found a minimal ''good'' basis set for SiO_2 (our results for this basis set are also given in Table II).

B. Effect of cluster size

We have also studied the dependence of vacancy formation energy on the cluster size for the 3–21G and 6–31G basis sets. The calculations performed for all four clusters demonstrate that the formation energy changes only within 0.5 eV. This is hardly surprising because the electron-density redistribution is localized preferentially on two Si ions and therefore the formation energy depends mainly on the lattice

relaxation. If the same number of atoms participates in the calculation of the lattice relaxation, the formation energy should depend insignificantly on the cluster size. A related issue concerns the effect of Si* ions on the relaxation. To check this we compared the displacements of the interface Si* atoms in cluster 1 with those of the corresponding Si atoms in cluster 3. The latter were treated as all-electron quantum-mechanical atoms. In both cases the displacements were calculated with respect to the corresponding fully relaxed nondefective structures. The absolute values of differences in displacements are quite small with the largest reaching 0.077 Å. These discrepancies can be made much smaller by more careful adjustment of the basis set and embedding potential.

C. Optical excitation energy

The optical transition energy is strongly affected by both the basis set and the cluster size. As the cluster size increases, the empty antibonding orbital associated with the vacancy moves into the group of empty levels representing the conduction band. This is due to the fact that the conduction-band width is increasing with cluster size and the corresponding states move as a function of the charge distribution in the cluster and its relaxation. Calculations of optical excitation energies in cluster 2 using the CIS method gives about 10 eV for the first strong transition localized near the vacancy. This effect has not been mentioned in previous publications due to the restricted atomic relaxation in Ref. 21, small clusters employed in Refs. 12–15, and the nature of MNDO method employed in Refs. 16–18, which does not allow proper description of the excited states. As has been pointed out in Ref. 12, neither the 6–31G basis set nor the CIS method is adequate for calculating optical properties of this defect due to importance of the electron correlation. We therefore expect that the electron correlation will strongly reduce the excitation energy. Indeed, the $S_0^* \rightarrow T_1$ transition energies calculated in cluster 1 and the 6–31G basis set using the coupled cluster method with single and double electron excitations are reduced by about 0.5 eV with respect to those calculated at the CIS level.

Finally we note that the vacancy relaxation in the excited triplet state T_1 in larger clusters is similar to that found in cluster 1. In particular, the Si-Si distance calculated in cluster 3 in the 6–31G basis set also increased to 3.36 Å after relaxation as in a small cluster 1. The calculated luminescence energies are all less than 1 eV.

VI. DISCUSSION

In this work we further developed the embedded cluster method[9–11] in order to study defects in ionic-covalent materials and applied it to the neutral oxygen vacancy in α-quartz. The improved embedding technique allowed us to perform a comprehensive analysis of the full extent and character of the lattice relaxation around this defect and to show that it induces very strong and anisotropic lattice distortion, which extends further than about 13 Å from the vacant site. We also predict the strong backward relaxation in the lowest triplet excited state of the vacancy (Fig. 6) and small luminescence energies. These results significantly alter the existing model of the neutral oxygen vacancy in SiO_2 as merely a symmetric displacement of the two silicon atoms towards each other due to formation of a chemical bond between them. They demonstrate that in spite of the rigidness of Si-O bonds the character of defect-induced lattice distortion in SiO_2 can be much more long range than intuitively anticipated and predicted in previous calculations. This should hold also for charged vacancy, peroxy linkage, and other defects in SiO_2. For comparison, the relaxation of atoms surrounding a neutral vacancy in some other oxides, such as ZrO_2 and MgO, is much smaller. In the case of MgO, ionic displacements are isotropic and at the distance of 8.0 Å from the neutral vacancy are less than 0.002 Å. A double positively charged anion vacancy in MgO produces a much stronger perturbation, but again, the displacements of the lattice ions decrease relatively rapidly and do not exceed 0.02 Å at the distance 8.0 Å from the vacancy. This results from different structure and chemical bonding in these materials. In particular, in MgO, unlike α-quartz, the oxygen site is the center of inversion. The peculiar structure of α-quartz is also manifested in the strong asymmetry of the relaxation of the two Si atoms neighboring the vacancy (Figs. 4–6).

Our results clearly demonstrate that defect parameters strongly depend on the extent of the lattice relaxation accounted for in calculations and on the cluster size and basis set. The vacancy formation energies calculated at the HF level in extended basis sets (see Table II) are broadly in agreement with those found by *ab initio* methods in Refs. 13–15, 20, 22 and 53, and also with those obtained by the MNDO method in Refs. 16–18. A meaningful quantitative comparison could be made with the results of Ref. 53 predicting 6.7 eV in the DZ+d basis set on both Si and O atoms. Our value of 6.08 eV in the 6–31G* basis set is predictably smaller due to a much larger relaxation energy. Taking further account of the electron correlation at the CI level with single and double excitations (CISD) increased the vacancy formation energy by 1 eV (for the 6–31G* basis set, cluster 1) in agreement with Ref. 53. Although further calculations are certainly needed to reach convergence, this should not affect our conclusion that formation of Si-Ge and Ge-Ge oxygen vacancies in quartz is energetically more profitable than Si-Si vacancies.

The calculations with extended basis sets show that the optical-absorption energy of the neutral vacancy in α-quartz should be larger than 5 eV. A more quantitative statement would be misleading due to the strong dependence of the results on parameters discussed above and on the method used for calculating the excited states. The small luminescence energy found in our calculations suggests that there is a high probability of a nonradiative $T_1^* \rightarrow S_0$ transition. A qualitatively similar result has been obtained in Refs. 13, 15, and 18. Therefore we expect that the luminescence of this defect will be strongly suppressed. We also predict that the double occupied energy level of the vacancy should be situated at about 2 eV above the top of the valence band. If we assume that the lowest optical excitation energy of the vacancy is 7.6 eV, its first excited state should be very close to

the bottom of the conduction band. Thus such excitation can result in the electron promotion into the conduction band and ionization of the vacancy.

Finally, we should note that the large radius of the lattice relaxation around the neutral vacancy in α-quartz found in this work should be characteristic to other defects, such as E' centers. The relaxation around these defects in amorphous silica is the subject of our current investigations and will be published separately. The radius of relaxation is comparable or even larger than the characteristic thickness of currently attainable oxide layers on silicon and dimensions of silica nanocrystals.[54] This suggests that properties of these defects may strongly depend on their position with respect to surfaces of respective systems. The strong lattice deformation and the dipole moment of neutral vacancies should affect their interaction. Our results suggest that this interaction could be affected by external electric field, which could be relevant for explaining the effects of poling of silica glass.[55]

ACKNOWLEDGMENTS

We are grateful to EPSRC (Grant No. GR/R01590/01) for financial support of this work. P.V.S. and A.L.S. would like to acknowledge the financial support from the U.S. Air Force and EOARD (Contract No. F61775-00-WE059). A.L.S. and A.M.S. are grateful to Fujitsu for support of their work. We are grateful to M. A. Szymanski and F. Lopez Gejo for valuable discussions and help in calculations, and to G. Pacchioni for useful comments.

APPENDIX: EXPRESSION FOR THE TOTAL ENERGY AS APPLIED TO SiO_2

For simplicity we attribute the interface Si* atoms to the quantum cluster. We will also draw no distinction between the classical atoms in region I and those in region II.

The total energy is given by

$$E = E_{\mathrm{qm}} + E_{\mathrm{cl}} + E_{\mathrm{ML}},$$

where E_{qm} is the total energy of the QM cluster in the potential of the classical environment, E_{cl} is the total energy of the classical environment, and E_{ML} is Mott-Littleton polarization energy of the crystal lattice outside region I.

The E_{qm} is a sum of the quantum-mechanical energy of the cluster in the external potential due to the environment V_{env} and classical correction term $W_{\mathrm{Si}^*,qm}$ describing the interaction of the interface Si* atoms with their O neighbors in the QM cluster. External potential $V_{\mathrm{env}} = V_{\mathrm{env}}^{\mathrm{Coul}} + V_{\mathrm{env}}^{\mathrm{short}}$ includes an electrostatic part and a short-range part; the latter is used to mimic the exchange and resonant contributions to the interaction energy:

$$E_{\mathrm{qm}} = \langle \Phi | H_0 + V_{\mathrm{env}}^{\mathrm{Coul}} | \Phi \rangle + V_{\mathrm{env}}^{\mathrm{short}} + W_{\mathrm{Si}^*,\mathrm{qm}},$$

where

$$H_0 = -\sum_i^{N_e} \frac{1}{2}\nabla^2 - \sum_i^{N_{\mathrm{qm}}} \sum_j^{N_e} \frac{Z_i}{|\mathbf{R}_i^{\mathrm{qm}} - \mathbf{r}_j|} + \sum_i^{N_e} \sum_j^{N_e} \frac{1}{|\mathbf{r}_i - \mathbf{r}_j|} + \sum_i^{N_{\mathrm{qm}}} \sum_j^{N_{\mathrm{qm}}} \frac{Z_i Z_j}{|\mathbf{R}_i^{\mathrm{qm}} - \mathbf{R}_j^{\mathrm{qm}}|} + \sum_i^{N_{\mathrm{Si}}} \hat{V}_i,$$

$$V_{\mathrm{env}}^{\mathrm{Coul}} = \sum_i^{N_{\mathrm{cor}}} \left(\sum_j^{N_e} \frac{Q_i^{\mathrm{cor}}}{|\mathbf{R}_i^{\mathrm{cor}} - \mathbf{r}_j|} + \sum_j^{N_{\mathrm{qm}}} \frac{Q_i^{\mathrm{cor}} Z_j}{|\mathbf{R}_i^{\mathrm{cor}} - \mathbf{R}_j^{\mathrm{qm}}|} \right) + \sum_i^{N_{\mathrm{she}}} \left(\sum_j^{N_e} \frac{Q_i^{\mathrm{she}}}{|\mathbf{R}_i^{\mathrm{she}} - \mathbf{r}_j|} + \sum_j^{N_{\mathrm{qm}}} \frac{Q_i^{\mathrm{she}} Z_j}{|\mathbf{R}_i^{\mathrm{she}} - \mathbf{R}_j^{\mathrm{qm}}|} \right),$$

$$V_{\mathrm{env}}^{\mathrm{short}} = \sum_i^{N_{\mathrm{qm}}} \sum_j^{N_{\mathrm{cl}}} W_{ij}^{\mathrm{Buck}}(\mathbf{R}_i - \mathbf{R}_j),$$

$$W_{\mathrm{Si}^*,\mathrm{qm}} = \sum_i^{N_{\mathrm{O}}} \sum_j^{N_{\mathrm{Si}^*}} W_{ij}^{\mathrm{Morse}}(\mathbf{R}_i - \mathbf{R}_j).$$

In the expressions above N_{qm} and N_e stand for the total number of atoms and electrons in the QM cluster, respectively (with $N_{\mathrm{Si}*}$ being the number of interface pseudo-Si atoms and N_0 the number of their quantum-mechanically treated oxygen neighbors), N_{cl} is the total number of classical atoms, N_{cor} and N_{she} are the total number of classical cores and shells, respectively, Z, Q^{cor}, Q^{she} are charges of nuclei in the QM cluster and of the classical cores and shells, respectively, $\mathbf{R}^{\mathrm{qm}}$ and $\mathbf{r}$ are coordinates of nuclei and electrons in the QM cluster, $\mathbf{R}^{\mathrm{cor}}$ and $\mathbf{R}^{\mathrm{she}}$ are coordinates of the classical cores and shells. The Hamiltonian H_0 includes the kinetic energy of the electrons, the electrostatic interaction of the electrons, and nuclei in the QM cluster (electron-nucleus, electron-electron, nucleus-nucleus), and an effective core potential for the interface Si* atoms. The external potential $V_{\mathrm{env}}^{\mathrm{Coul}}$ includes interaction of classical cores and shells with the electrons and nuclei of the QM cluster. The terms $V_{\mathrm{env}}^{\mathrm{short}}$ and $W_{\mathrm{Si,qm}}$ are both represented by pairwise Buckingham or Morse-type classical potentials.

The total energy of the classical region is given by

$$E_{\mathrm{cl}} = \sum_i^{N_{\mathrm{cl}}} W_i^{\mathrm{spring}} + \sum_i^{N_{\mathrm{cl}}} \sum_{j \neq i}^{N_{\mathrm{cl}}} (W_{ij}^{\mathrm{Coul}} + W_{ij}^{\mathrm{Buck}}),$$

where

$$W_i^{\mathrm{spring}} = \frac{k_i}{2} |\mathbf{R}_i^{\mathrm{cor}} - \mathbf{R}_i^{\mathrm{she}}|^2$$

and

$$W_{ij}^{\mathrm{Coul}}=\frac{Q_i^{\mathrm{cor}}Q_j^{\mathrm{cor}}}{|\mathbf{R}_i^{\mathrm{cor}}-\mathbf{R}_j^{\mathrm{cor}}|}+\frac{Q_i^{\mathrm{cor}}Q_j^{\mathrm{she}}}{|\mathbf{R}_i^{\mathrm{cor}}-\mathbf{R}_j^{\mathrm{she}}|}+\frac{Q_i^{\mathrm{she}}Q_j^{\mathrm{cor}}}{|\mathbf{R}_i^{\mathrm{she}}-\mathbf{R}_j^{\mathrm{cor}}|}+\frac{Q_i^{\mathrm{she}}Q_j^{\mathrm{she}}}{|\mathbf{R}_i^{\mathrm{she}}-\mathbf{R}_j^{\mathrm{she}}|}.$$

In the above W^{spring} is the polarization energy of the atoms in the electrostatic field due to the defect (k is related to the polarizability of ions in the crystal), W^{Coul} is the electrostatic energy of the cores and shells of all pairs of classical atoms, W^{Buck} is the pairwise atomic interactions represented using classical Buckingham-type potentials.

[1] L. Skuja, J. Non-Cryst. Solids **239**, 16 (1998).

[2] *Defects in* SiO_2 and *Related Dielectrics: Science and Technology*, edited by G. Pacchioni, L. Skuja, and D. L. Griscom (Kluwer, Dordrecht, 2000), p. 624.

[3] B. Poumellec and F. Kherbouche, J. Phys. III **6**, 1595 (1996).

[4] A. Othonos and K. Kalli, *Fiber Bragg Gratings* (Artech House, Boston-London, 1999).

[5] V. B. Sulimov and V. O. Sokolov, in *Advances in Fibre Optics, Proceedings of SPIE*, edited by E. M. Dianov (SPIE, Bellingham, 2000), Vol. 4083, p. 158.

[6] W. B. Fowler and A. H. Edwards, Radiat. Eff. Defects Solids **146**, 11 (1998).

[7] *Structure and Imperfections in Amorphous and Crystalline Silicon Dioxide*, edited by R. A. B. Devine, J.-P. Duraud, and E. Dooryhée (John Wiley & Sons Ltd., Chichester, 2000), p. 505.

[8] L. Skuja, in *Defects in* SiO_2 *and related dielectrics: Science and technology* (Ref. 2), p. 73.

[9] A. L. Shluger, P. V. Sushko, and L. N. Kantorovich, Phys. Rev. B **59**, 2417 (1999).

[10] P. V. Sushko, A. L. Shluger, and C. R. A. Catlow, Surf. Sci. **450**, 153 (2000).

[11] P. V. Sushko, A. L. Shluger, R. C. Baetzold, and C. R. A. Catlow, J. Phys.: Condens. Matter **12**, 8257 (2000).

[12] B. B. Stefanov and K. Raghavachari, Phys. Rev. B **56**, 5035 (1997).

[13] G. Pacchioni, A. M. Ferrari, and G. Ieranò, Faraday Discuss. **106**, 155 (1997).

[14] G. Pacchioni and G. Ieranò, Phys. Rev. B **57**, 818 (1998).

[15] G. Pacchioni and A. Basile, J. Non-Cryst. Solids **254**, 17 (1999).

[16] V. B. Sulimov, C. Pisani, F. Corà, and V. O. Sokolov, Solid State Commun. **90**, 511 (1994).

[17] V. B. Sulimov and V. O. Sokolov, J. Non-Cryst. Solids **191**, 260 (1995).

[18] V. B. Sulimov, V. O. Sokolov, and B. Poumellec, Phys. Status Solidi B **196**, 175 (1996).

[19] K. C. Snyder and W. B. Fowler, Phys. Rev. B **48**, 13 238 (1993).

[20] D. Erbetta, D. Ricci, and G. Pacchioni, J. Chem. Phys. **113**, 10 744 (2000).

[21] V. B. Sulimov, S. Casassa, C. Pisani, J. Garapon, and B. Poumellec, Modell. Simul. Mater. Sci. Eng. **8**, 763 (2000).

[22] A. Oshiyama, Jpn. J. Appl. Phys., Part 2 **37**, L232 (1998).

[23] M. Boero, A. Pasquarello, J. Sarntheim, and R. Car, Phys. Rev. Lett. **78**, 887 (1997).

[24] P. E. Blöchl, Phys. Rev. B **62**, 6158 (2000).

[25] Q. S. Wang and N. A. W. Holzwarth, Phys. Rev. B **41**, 3211 (1990).

[26] B. Králik, E. K. Chang, and S. G. Louie, Phys. Rev. B **57**, 7027 (1998).

[27] A. S. Foster, V. B. Sulimov, F. L. Gejo, A. L. Shluger, and R. M. Nieminen, Phys. Rev. B **64**, 224108 (2001).

[28] C. M. Carbonaro, V. Fiorentini, and S. Missidda, J. Non-Cryst. Solids **221**, 89 (1997).

[29] D. C. Allan and M. P. Teter, J. Am. Ceram. Soc. **73**, 3247 (1990).

[30] N. Capron, S. Carniato, A. Lagraa, and G. Boureau, J. Chem. Phys. **112**, 9543 (2000).

[31] N. Capron, S. Carniato, G. Boureau, and A. Pasturel, J. Non-Cryst. Solids **245**, 146 (1999).

[32] G. Boureau and S. Carniato, Solid State Commun. **98**, 485 (1996).

[33] J. Sauer, Chem. Rev. **89**, 199 (1989).

[34] A. L. Shluger and J. D. Gale, Phys. Rev. B **54**, 962 (1996).

[35] B. G. Dick and A. W. Overhauser, Phys. Rev. **112**, 90 (1958).

[36] B. W. H. van Beest, G. J. Kramer, and R. A. Van Santen, Phys. Rev. Lett. **64**, 1955 (1991).

[37] These techniques have been reviewed in a special issue: J. Chem. Soc., Faraday Trans. 2 **85**, 335 (1989), edited by C. R. A. Catlow and A. M. Stoneham.

[38] J. D. Gale, J. Chem. Soc., Faraday Trans. **93**, 69 (1997).

[39] J. M. Vail, J. Phys. Chem. Solids **51**, 589 (1990).

[40] A. L. Shluger, A. H. Harker, V. E. Puchin, N. Itoh, and C. R. A. Catlow, Modell. Simul. Mater. Sci. Eng. **1**, 673 (1993).

[41] P. V. Sushko, J. L. Gavartin, and A. L. Shluger, J. Phys. Chem. B **106**, 2269 (2002).

[42] A. E. Reed, R. B. Weinstock, and F. Weinhold, J. Chem. Phys. **83**, 735 (1985).

[43] B. Civalleri, C. M. Zicovich-Wilson, P. Ugliengo, V. R. Saunders, and R. Dovesi, Chem. Phys. Lett. **292**, 394 (1998).

[44] GAUSSIAN98 (edition A7), M. J. Frisch, G. W. Trucks, H. B. Schlegel, G. E. Scuseria, M. A. Robb, J. R. Cheeseman, V. G. Zakrzewski, J. A. Montgomery, R. E. Stratmann, J. C. Burant, S. Dapprich, J. M. Millam, A. D. Daniels, K. N. Kudin, M. C. Strain, O. Farkas, J. Tomasi, V. Barone, M. Cossi, R. Cammi, B. Mennucci, C. Pomelli, C. Adamo, S. Clifford, J. Ochterski, G. A. Petersson, P. Y. Ayala, Q. Cui, K. Morokuma, D. K. Malick, A. D. Rabuck, K. Raghavachari, J. B. Foresman, J. Cioslowski, J. V. Ortiz, B. B. Stefanov, G. Lui, A. Liashenko, P. Piskorz, I. Komaromi, R. Gomperts, R. L. Martin, D. J. Fox, T. Keith, M. A. Al-Laham, C. Y. Peng, A. Nanayakkara, C. Gonzalez, M. Challacombe, P. M. W. Gill, B. G. Johnson, W. Chen, M. W. Wong, J. L. Andres, M. Head-Gordon, E. S. Replonge, and J. A. Pople (Gaussian Inc., Pittsburgh, 1998).

[45] V. B. Neustruev, J. Phys.: Condens. Matter **6**, 6901 (1994).

[46] H. B. Jansen and P. Ross, Chem. Phys. Lett. **3**, 140 (1969).

[47] A. Hamza, Á. Vibók, G. J. Halász, and I. Mayer, J. Mol. Struct.: THEOCHEM **501–502**, 427 (2000).

[48] J. B. Foresman, M. Head-Gordon, and J. A. Pople, J. Phys. Chem. **96**, 135 (1992).

[49] R. J. Rico and M. Head-Gordon, Chem. Phys. Lett. **213**, 224 (1993).
[50] D. Griscom and M. Cook, J. Non-Cryst. Solids **182**, 119 (1995).
[51] J. K. Rudra and W. B. Fowler, Phys. Rev. B **35**, 8223 (1987).
[52] R. H. Bartram and A. M. Stoneham, Solid State Commun. **17**, 1593 (1975).
[53] G. Pacchioni and G. Ieranò, Phys. Rev. B **56**, 7304 (1997).
[54] A. S. Zyubin, Yu. D. Glinka, A. M. Mebel, A. H. Lin, L. P. Hwang, and Y. T. Chen, J. Chem. Phys. **116**, 281 (2002).
[55] R. A. Mayers, N. Mukherjee, and S. R. J. Brueck, Opt. Lett. **16**, 1732 (1991).